Initial Polymerization Reactions in Particle-Forming Ar/He/C_2H_2 Plasmas Studied via Quantitative Mass Spectrometry

A. Consoli, J. Benedikt,* and A. von Keudell

Research Group Reactive Plasmas, Ruhr-Universität Bochum, 44780 Bochum, Germany

Received: May 13, 2008; Revised Manuscript Received: August 9, 2008

The initial polymerization reactions in particle forming Ar/He/C_2H_2 plasmas are studied using molecular beam mass spectrometry (MBMS). The measured mass spectra are disentangled and quantified with the help of Bayesian probability theory. This approach uses the measured mass spectra and the cracking patterns (CPs) of the species that are formed in the plasma as the main input parameter. The CPs are either taken from calibration measurements or the NIST database or estimated based on a comparison to CPs of similar molecules. These estimated CPs are then modified by Bayesian analysis to fit the measured data. The CPs of C_6H_2, C_6H_4, and C_8H_2, which are not available in the NIST database, are determined in this way and can serve as good estimation until precise data is published. The temporal evolution after plasma ignition of the densities of in total 22 species (hydrocarbons, noble gases, and impurities) are quantified and expressed as partial pressures. The most abundant products in our plasma are C_4H_2 and C_6H_2 molecules with maximum partial pressures of 0.1 and 0.013 Pa, respectively. Our quantitative data can be used to validate plasma chemistry models. First comparison is made to a plasma chemistry model of similar C_2H_2 plasma already available in the literature. The comparison indicates that dissociative electron attachment to $C_{2n}H_2$ ($n > 1$) molecules is a dominant source of negative ions in C_2H_2 plasmas. Additionally, the C_2H_4 has been identified as a precursor for C_nH_4 molecules.

I. Introduction

The formation of dust particles is a common phenomenon in many reactive plasmas from, i.e., silane or acetylene. In the past, such particles were considered an undesired byproduct for most plasma processes in the semiconductor industry because they induce defects on the processed wafers.[1,2] However, in the meantime, beneficial applications of plasma-produced particles have also been identified. Especially, particles with diameters smaller than 10 nm exhibit unique electrical and optical properties and may serve as quantum dots in electronic circuits or as photonic devices.[3] Furthermore, if small particles are embedded in an amorphous silicon matrix, they can improve the electronic properties of silicon thin film solar cells.[4] Finally, plasma-produced particles serve also as astroanlagoues[5] to study reactions in star formation on a laboratory scale.

Dust particle formation occurs in four consecutive reaction steps as being resolved by Perrin and Hollenstein:[6] (i) first, primary clusters are formed by neutral−neutral or neutral−anion reactions; (ii) second, nucleation of clusters by avalanche condensation occurs and small particles are created with radii $r_p < 5$ nm; (iii) third, coagulation or agglomeration into macroscopic particles ($r_p < 50$ nm) takes place; (iv) finally, negatively charged particles grow further by condensation, e.g., surface aggregation by radical attachment.

The initial reaction steps are best studied for silane plasmas. The most important precursor for dust formation are either silyl (SiH_3^-) or silylene (SiH_2^-) anions.[7−9] Both anions polymerize with the feed gas silane, but the silyl anion pathway dominates the formation of larger anions.

Such detailed knowledge on the initial reaction steps does not exist for acetylene plasmas used for dust production. In analogy to SiH_4 plasmas, the C_2H^- anion has been proposed as precursor.[10] However, no direct evidence for this hypothesis is available. Actually, a recent model calculation of De Bleecker et al.[9] with the C_2H^- anion as the only negative ion shows a strong disagreement between the predicted negative ion spectrum compared to actual experimental data measured by Deschenaux et al.[11] Apparently, more reaction channels and precursors need to be considered.

We studied the formation of dust particles in capacitively or inductively coupled plasmas from argon/helium/acetlyne mixtures in the past.[12,13] It was shown that particle formation is a very fast process reaching particle diameters of 2−10 nm already after 250 ms. To cover the complete growth sequence of particles reaching diameters of several 100 nm, the evolution of the plasma chemistry over several seconds need to be analyzed.

To investigate this initial stage of dust particle formation in C_2H_2-containing plasmas, we have applied molecular beam mass spectrometry (MBMS) to measure the temporal evolution of absolute neutral species densities. In our previous work, we focused on a qualitative analysis of stable reaction products in an Ar/He/C_2H_2 capacitively coupled plasma (CCP).[14] Chemistry pathways leading to the production of various hydrocarbon products were suggested. In this paper, Bayesian statistics will be used for a quantitative analysis of the reaction products in C_2H_2-containing plasmas. The central goal is to compare these quantitative data with the recent model of de Bleecker et al.[9,15] Such a validation is more robust if many species are quantified simultaneously. This is exactly fulfilled in our approach using mass spectrometry in which 22 species are quantified.

II. Experimental Section

The plasma experiments are performed in a stainless steel vessel similar to a GEC reference cell with 6 cm electrode

* To whom correspondence should be addressed. E-mail: Jan.Benedikt@rub.de.

10.1021/jp8042413 CCC: $40.75
Published on Web 10/22/2008

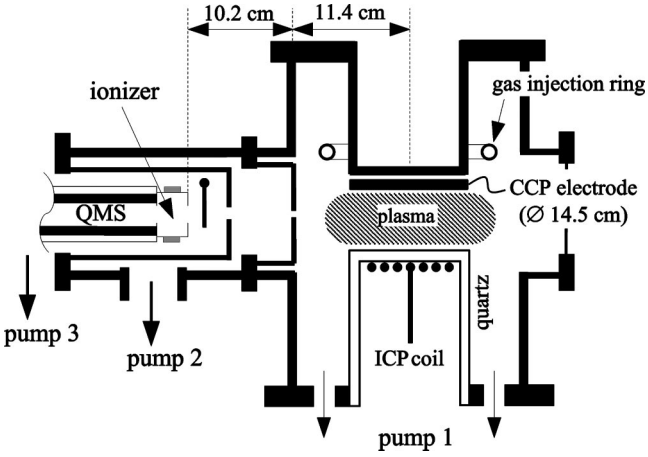

Figure 1. Experimental setup.

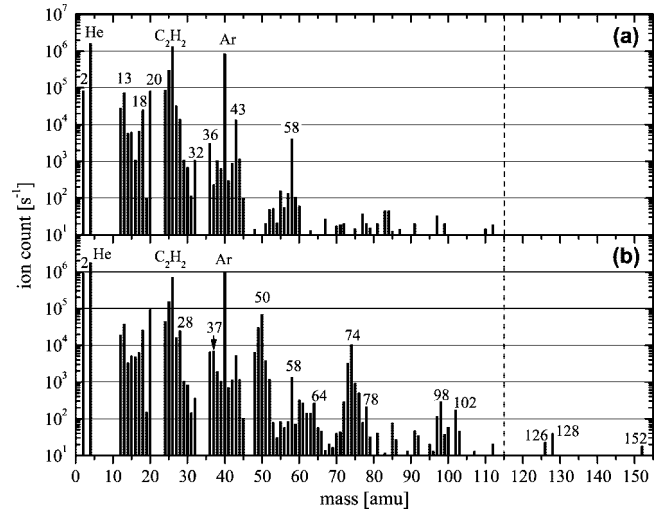

Figure 2. Reconstructed mass spectra prior to plasma ignition (a) and 1 s after plasma ignition (b).

spacing and 14.5 cm electrode diameter. A scheme of the setup is shown in Figure 1. The top electrode is powered and a capacitively coupled plasma is generated between the electrodes. Particles are generated with a prepared gas mixture of Ar (4 sccm), He (15 sccm) and C_2H_2 (4 sccm). A forward power of $P = 80$ W is used. The pressure without plasma is 6 Pa and after plasma ignition, it drops to ca. 4 Pa due to acetylene consumption. After $\Delta t = 8$ s, the C_2H_2 gas flow is switched off.

Time resolved molecular beam mass spectrometry (MBMS) is used to follow the neutral gas phase chemistry. We use a Balzers HiQuad mass spectrometer QMG 700 (mass range up to 2048 amu), which is separated from the chamber by a two stage differential pumping system. The pressure in the second stage housing the mass spectrometer is around 3×10^{-7} mbar during the measurements. A molecular beam is sampled from the chamber through a sampling orifice with a diameter of 0.6 mm and a distance of 114 mm from the reactor axis. The line-of-sight distance between the first orifice and the ionizer of the mass spectrometer is 102 mm. The mass dependence of the transmission function of the spectrometer is calibrated by measuring noble gases and a few other gases at known pressure. All mass spectra are corrected accordingly. More details can be found in ref 14.

A step scan procedure for recording mass spectra during the plasma experiment is used:[14] during one plasma experiment, the temporal evolution of two masses is followed (scan). The first mass is always the molecular mass of C_2H_2 (26 amu), that is used as time reference signal and for reproducibility control. The second mass is a selected mass of interest. This procedure is repeated with the next mass channel (step) in another plasma experiment under identical experimental conditions. All possibly contributing mass channels to hydrocarbon mass spectra up to 115 amu and selected mass channels between 116 and 152 amu are investigated. The step scan procedure yields a time resolution of 100 ms or less for the mass spectra. Two reconstructed mass spectra are exemplarily shown in Figure 2: (a) prior to plasma; (b) 1 s after plasma ignition.

A quantification of mass spectra is only possible if calibration experiments are performed simultaneously. For this, the species of interest are prepared in the chamber at a fixed pressure and with fixed butterfly valve. The species are then monitored by the mass spectrometer yielding a calibration spectrum. The absolute pressure is measured by a capacitance gauge. As a result, the absolute pressure can be correlated to a count rate in the calibration spectrum, which is used later to extract partial pressures of the species in the plasma. Such calibration scheme works only for stable species, which can easily be prepared at a known pressure in the system, namely CH_4, C_2H_2, C_2H_4, Ar, N_2, and O_2. The calibration of C_2H_2 takes the main impurities acetone and C_2H_4 into account as discussed below. The quantification of other species is achieved by a relative calibration scheme based on a comparison of ionization cross sections as will be described below.

To account for background species in the chamber/mass spectrometer, a background spectrum is taken shortly after or before any calibration measurement. The subtraction of the background spectrum from the calibration data yields the actual calibration spectrum.

III. Data Analysis

Mass spectra are often analyzed in a nonquantitative manner by directly interpreting raw signal peaks. However, this method can be misleading since the raw signals refer to ions, which are produced from stable neutrals via fragmentation and ionization in the ionizer of the mass spectrometer. Consequently, any quantification is difficult because the efficiency of this ionization depends sensitively on the identity of the stable neutral of interest. This is usually resolved by a conventional two step approach: first, the fragmentation itself expressed as the so-called cracking pattern (CP) is determined, either from databases or by direct calibration experiments. Second, the CP of a given species s is rescaled by constant factor f_s and is subtracted from the raw data until the contribution of this single species to the mass spectrum is eliminated. This factor f_s is proportional to the product of species concentration or partial pressure and ionization efficiency in the ionizer of the mass spectrometer. The second step is repeated until all peaks in the mass spectrum are accounted for. The factors f_s are then a measure for the contribution of species$s$to the gas mixture. The main disadvantage of this procedure is error propagation during consecutive subtractions rendering the factors f_s very unreliable. A typical consequence are solutions exhibiting negative species densities.

This limitation of a conventional analysis is resolved using Bayesian statistics, which combines consistently CP, mass spectra and, all corresponding errors in a single analysis. Details of this approach are presented by Schwarz-Selinger et al.[16] and by Kang et al.[17] The most important steps are described in Appendix A. Briefly, the general mass spectra problem can be presented as

$$\vec{d} = \hat{C}\vec{x} \quad (1)$$

Here, the vector $\vec{d}$ contains the mass spectrum data, the matrix $\hat{C}$ contains the CPs of each species present in the experiment, and the vector $\vec{x}$ contains the concentrations of these species. In Bayesian analysis, this equation is transformed into a more suited description, which covers all available input data including experimental errors. In this way, by means of a Markov chain Monte Carlo (MCMC) algorithm, a set of data is found containing the input data and concentrations with the largest probability of being a solution to the problem. The resulting concentrations of species ($\vec{x}$) are then converted to partial pressures with the help of calibration measurements or, if these were not available, by means of comparing total ionization cross sections.

In the fitting process of Bayes analysis the prior CPs are modified, yielding posterior CPs, to obtain a better solution of the problem. If the prior CPs are accurate (i.e., from calibration measurements), the prior and posterior CPs will be almost identical. Otherwise a large discrepancy can result between both CPs. This allows the implementation of unknown CPs by estimating the prior CP of a species, supposed to be present in the plasma, and comparing it to the corresponding posterior CP. Unreasonable changes in the CP indicate that the species is not present in the plasma. This approach is not possible in the conventional analysis.

Most crucial to the Baysian approach is the selection of input data and determination of corresponding error margins. The more information is known, i.e., prior CPs of all species present in the discharge, the more precise will be the resulting partial pressures. For example, the prior CPs can be either measured or can be taken from a database. For some species both of these options were not possible. Therefore, we have estimated the spectra based on similar molecules, which are supposed to have also similar mass spectra (cf. IV B). In order to understand the Bayes results (concentrations/partial pressures, posterior CPs), it is important to consider which input data is applied in the analysis and how this data is obtained. This information is also vital for validating plasma chemistry models. All our input data will be explained in detail in the next section.

IV. Input Data for Bayes Analysis

The input data for the Bayesian analysis are (i) reconstructed mass spectra, (ii) 22 prior CPs, either obtained from calibration measurements, from the NIST[18] database, or by estimation, and (iii) the calibration pressures and total ionization cross sections σ for each species. All data include an experimental or estimated error. Table 1 provides a summary of all input data.

A. Reconstructed Mass Spectra. The data $\vec{d}$ correspond to 29 mass spectra covering the whole plasma phase starting from 0.2 s until 4.5 s after plasma ignition. The time steps between the spectra are 0.1 and 0.2 s in regions of strong signal gradients and 0.5 s otherwise. The experimental errors are the statistical error of the count rates of each peak in the spectra.

B. Prior Cracking Patterns (CPs). The selection of the species that are believed to be present in the plasma defines the set of necessary CPs. Based on previous work,[14] in which we qualitatively identified dominant hydrocarbons and residual background gases, we have included a selection of up to 22 species with corresponding CPs having masses up to 103 amu.

No hydrocarbons with masses larger than 103 amu are considered in the analysis because the signal intensities at these mass channels are very low. Nevertheless, larger hydrocarbons may contribute to signals at lower masses. In the Bayesian analysis, this additional signal may cause an overestimation of the densities of smaller hydrocarbons. Moreover, it is still possible that some other smaller molecules (e.g., isomers) not implemented in our Bayes analysis contribute to the measured mass spectra. To check for the sensitivity of our analysis to "missing" species, the effect of arbitrarily adding or removing the CPs of C_3H_4 (propyne), of C_3H_6 (propene), and of linear C_6H_6 (1,5-/2,4-hexadiyne) on the partial pressures have been tested. The results have shown that almost all CPs and partial pressures stay the same, except that of C_5H_4 (posterior CP and partial pressure affected) and of C_6H_6 (partial pressure affected). Apparently, the possible contribution of some missing hydrocarbons does not alter the densities and CPs of hydrocarbons included in our analysis. The final set of selected species is shown in Table 1.

TABLE 1: Input Parameters for Bayes Analysis[a]

species	structure	cracking pattern	σ [10^{-16} cm^{-2}]
CH_4 (methane)	CH_4	calibrated	
C_2H_2 (acetylene)	HCCH	calibrated	4.4
C_2H_4 (ethylene)	H_2CCH_2	calibrated	
C_3H_4 (propyne)	H_3CCCH	NIST	7.7
C_3H_6 (propene)	$H_3CCH_2CH_3$	NIST	8.7
C_4H_2 (1,3-butadiyne)	HCCCCH	NIST	8.9
C_4H_4 (1-buten-3-yne)	$H_2CCHCCH$	NIST	9.9
C_5H_4 (1,3-pentadiyne)	CH_3CCCCH	estimated	11.4 (add.)
C_6H_2 (1,3,5-hexatriyne)	HCCCCCCH	estimated	13
C_6H_4	$H_2CCCCCCH_2$	estimated	13.2 (add.)
C_6H_6 (benzene)	aromatic	NIST	15
C_6H_6 (1,5 hexadiyne)	linear	NIST	15
C_6H_6 (2,4 hexadiyne)	linear	NIST	15
C_8H_2 (1,3,5,7-octatetrayne)	HCCCCCCCCH	estimated	16.3
C_8H_6 (phenylacetylene)	aromatic	NIST	17.7 (add.)
C_3H_6O (acetone)		NIST/calibrated*	9.5 (est.)
Ar		calibrated	
N_2		calibrated	
O_2		calibrated	
H_2O		calibrated*	2.3
CO_2		NIST	3.3
CO		NIST	2.5

[a] Given are the species and structures, the method how the species cracking patterns are obtained, and the applied total electron-impact ionization cross sections σ at 70 eV. No calibration pressure information is available for calibrated cracking patterns marked with *. Cross sections are taken from the NIST databse[19] if not otherwise indicated, retrieved by additivity rules (add.), or estimated (est.).

Several methods have been applied to determine the prior CPs:

1. ***CPs from Calibration Measurements.*** The most accurate prior CPs are obtained in direct calibration measurements of species at known absolute pressure. Such calibration measurements were performed for CH_4, C_2H_2, C_2H_4, Ar, N_2, and O_2.

A similar calibration measurement without total pressure information was performed for H_2O and acetone (C_3H_6O). A small amount of H_2O is always present in the chamber and in the mass spectrometer and can be easily detected in a background scan without any feed gases. Acetone is often used as solvent for C_2H_2 in gas bottles. The acetone CP is derived from a comparison of the data for C_2H_2 dissolved in acetone with that for solvent-free C_2H_2. Unfortunately, only the highest intensity peaks are visible. Smaller intensity peaks are covered by C_2H_2 intensity peaks. Those smaller peaks are estimated from a comparison with acetone spectra from the NIST database. The experimental errors in the calibration spectra are given by the statistical error of the count rates in each spectrum.

The calibration of C_2H_2 requires its main impurities acetone and C_2H_4 be taken into account, which we have identified in

the course of the analysis. This is achieved by using also the Bayes algorithm, to eliminate the contributions of C_2H_4 and of acetone from the C_2H_2 calibration spectrum.

2. *CPs from NIST.* The prior CPs were taken from the NIST (National Institute of Standards and Technology) database[18] if a calibration measurement was not possible. The CPs in the database are normalized and contain no error margins. In general, these CPs are accurately measured and very reliable but may contain systematic errors, such as a missing correction for the mass transmission of the spectrometer. The CPs of C_3H_4 (propadiene), of C_3H_6 (propene), of C_4H_2 (1,3-butadiyne), of C_4H_4 (1-buten-3-yne), of C_6H_6 (benzene), of C_8H_6 (phenylacetylene), of CO, and of CO_2 were selected. Estimated error margins for these data are based on the suggestions in ref 17. They are set to 10% of the peak height. In addition, a lower limit for the errors is assumed being at least 1% of the height of the highest peak in the CP.

The selection of proper CPs for larger hydrocarbons is difficult because several isomers with either single, double, or triple bonds usually exist. This ambiguity is reduced by assuming that the triple bond of acetylene is preserved in the plasma chemistry. In addition, linear C_6H_6 (1,4- and 2,4-hexadiyne), aromatic C_6H_6 (benzene), and aromatic C_8H_6 (phenylacetylene) have been included and tested in the analysis.

3. *CPs from Estimation.* The prior CPs were estimated if no calibration measurements were possible and no literature values were available. This holds for C_5H_4, C_6H_2, C_6H_4, and C_8H_2.

This estimation is based on a comparison to similar molecules with known CPs, as it is illustrated for C_6H_2: first, the molecule C_4H_2 with its CP from the NIST database is taken as a model. The part of the CP around mass 50 amu in the C_4H_2 spectrum is used as an estimate for the part of the CP at mass 74 amu in the C_6H_2 spectrum. This part is assumed to exhibit maximum intensity because dissociative ionization leads mainly to the loss of only one or two hydrogen atoms. Second, an additional fragmentation peak is added at mass 61 amu to account for the formation of C_5H by the cracking of the triple bond of C_6H_2 in the ionizer. Such a reaction is similar to the formation of C_3H from C_4H_2. According to that reaction, an intensity of 5% of the absolute maximum peak at mass 74 amu is adopted. Third, similar considerations are made for other parts of the fragmentation pattern corresponding to the formation of C_4H, C_3H, C_2H, and CH.

This method of estimation is performed for all other species with C_5H_6 being the model for C_5H_4, C_4H_2 being the model for C_6H_2, C_6H_4, and C_8H_2. The input CPs are shown below together with the posterior CPs produced by the Bayes analysis.

The huge advantage of using Bayesian statistics is the fact that the accuracy of the input data is accounted for by using individual error margins. Therefore, the initial error margins of these estimated CPs is set to very high values between 50% to 100% of the peak height. These large errors allow the Bayes algorithm to alter these cracking patterns/peak heights to fit the experimental data.

It is important to note that the proper choice of error margins is key to the whole analysis process. Large error margins underestimate the quality of the data and waste therefore information, whereas too small error margins generate large discrepancies between the fit and the experimental data.

C. Total Electron-Impact Ionization Cross Sections and Calibration Pressures. Total electron-impact ionization cross sections at 70 eV (electron energy used in the ionizer of the mass spectrometer) and calibration pressures are given in Table 1. Calibration pressures are only available for CH_4, C_2H_2, C_2H_4, Ar, N_2, and O_2. Therefore, total ionization cross sections for the remaining species and that of the reference molecule C_2H_2 are required. Most of these data are retrieved from the NIST database, in which a binary encounter Bethe model was applied.[19] In this way, total electron-impact ionization cross section are calculated for C_2H_2, C_3H_4 (propyne), C_3H_6, C_4H_2, C_4H_4, C_4H_6, C_6H_2, C_6H_4, C_6H_6 (benzene), CO, and CO_2.

The total electron-impact ionization cross sections of C_5H_4, of C_6H_4, and of C_8H_6 are not listed in this database. We use, therefore, additivity rules to estimate these data.[20] The additivity rules describe the fact that the total electron impact ionization cross section of hydrocarbons scales approximately with the number of C—C, C—H, C═C, and C≡C bonds (see Figure 6) at electron energies higher than 30 eV. From such scaling, the unknown ionization cross sections are derived, as given in Table 1.

In addition, no ionization cross section for acetone $\sigma_{acetone}$ is available. Therefore, we estimated it to $\sigma_{acetone} = 9.5 \times 10^{-16}$ cm^{-2} as being composed of the known cross sections of C_3H_6 and a half of the CO_2 cross section. A systematic error for the absolute concentration of acetone of several 10% is assumed.

V. Results and Discussion

The analysis of the temporal evolution of the mass spectra as taken during the initial phase of particle formation in an Ar/He/C_2H_2 plasma are presented in the following. For this analysis, all mass spectra, covering the first 4.5 s after plasma ignition, a given set of prior CPs and error margins are combined in a single analysis. The corresponding MCMC-algorithm requires several hours computational time on a standard PC to find a saturating solution.

Since all data are simultaneously considered in one analysis, the results are very robust with respect to possible errors in single data vectors. In addition, the temporal evolution of the mass spectra resulting from a complex chemistry of many species represents a restrictive and informative data set, which allows a quantitative determination of CPs and partial pressures because all data are combined in a single analysis. In contrast, the quantification of 22 species based on the analysis of only one single mass spectrum is, especially in the case if some CPs are only estimated, impossible.

The Bayesian analysis yields two types of output data: (i) posterior CPs and (ii) the temporal evolution of species concentrations as being formed during the initial phase of particle formation.

A. Cracking Patterns (CPs). Figures 3−5 compare prior (bars) with posterior (dots with error bars) CPs. All CPs are scaled to a maximum peak relative intensity of 1000. The results are discussed with respect to the different quality of the information that is used to define the prior CPs.

1. Prior CPs from Calibration Experiments. Figure 3 shows the CPs of calibrated hydrocarbons CH_4, C_2H_2, and C_2H_4. The prior and posterior CPs agree very well. The very small error margins indicate the good knowledge of these CPs. Such a good agreement is usually achieved if calibration measurements are available. As a consequence, the partial pressures of those species are the most accurate.

2. Prior CPs from the NIST Database. Figure 4 shows the prior CPs of C_4H_2, C_4H_4, C_6H_6 (benzene), and C_8H_6 (phenylacetylene) taken from the NIST database and the corresponding posterior CPs. The main peaks of the prior and posterior CPs of C_4H_2 agree very well. Only differences at mass channels 25 amu and below are visible, corresponding to C_2H, C_2, CH, and

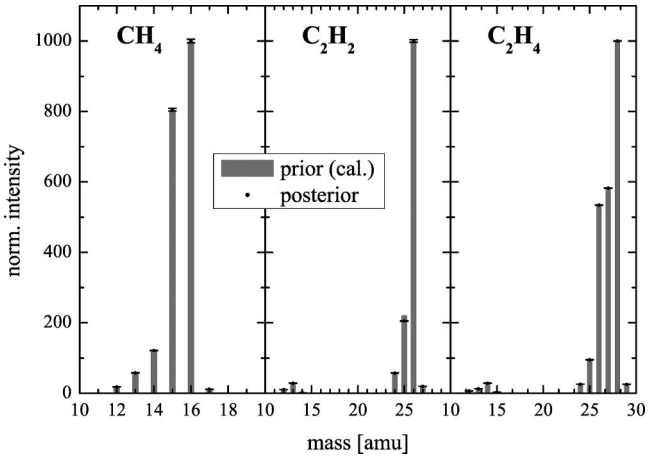

Figure 3. Prior and posterior CPs of CH_4, C_2H_2, and C_2H_4. The prior CPs are determined in calibration measurements.

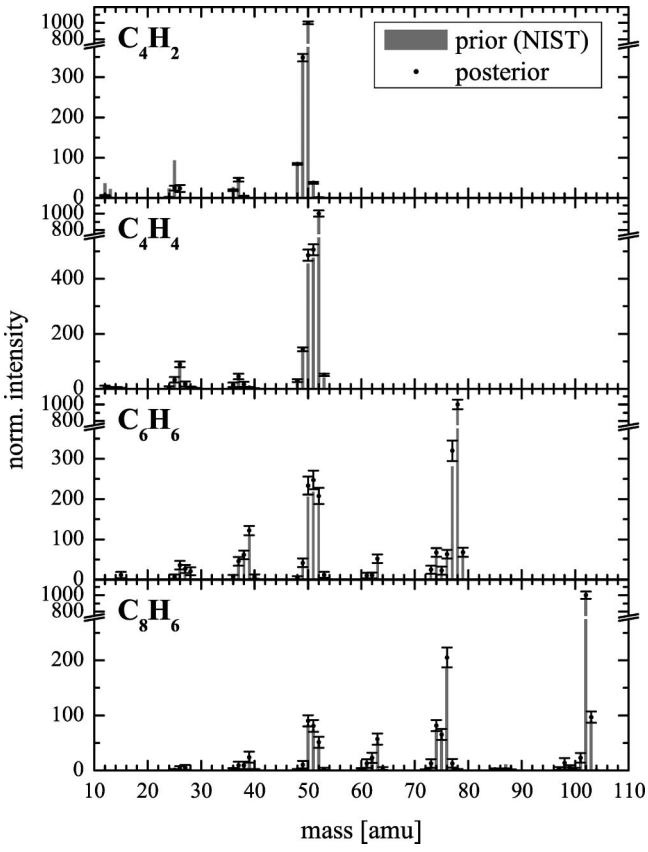

Figure 4. Prior and posterior CPs for C_4H_2, C_4H_4, C_6H_6, and C_8H_6. The prior CPs are taken from the NIST database.

C. These fragments are formed from almost any hydrocarbon entering the mass spectrometer, resulting in a massive overlap of CPs, which induces larger posterior errors. The deviation at small masses might also be caused by an uncorrected mass transmission of the spectrometer that is used for the acquisition of the C_4H_2 NIST spectrum.

The posterior CPs C_4H_4, C_6H_6 (benzene), and C_8H_6 (phenylacetylene) as shown in Figure 4 agree very well with the prior CPs from NIST. However, the selection of C_6H_6 is not conclusive. The results of linear C_6H_6 (1,5- and 2,4-hexadiyne), not shown here, agree well with the corresponding prior, as well. Both linear and polycyclic C_6H_6 are compatible with the measured data. On the other hand, the presence of aromatic molecules seems reasonable because aromatic molecules are

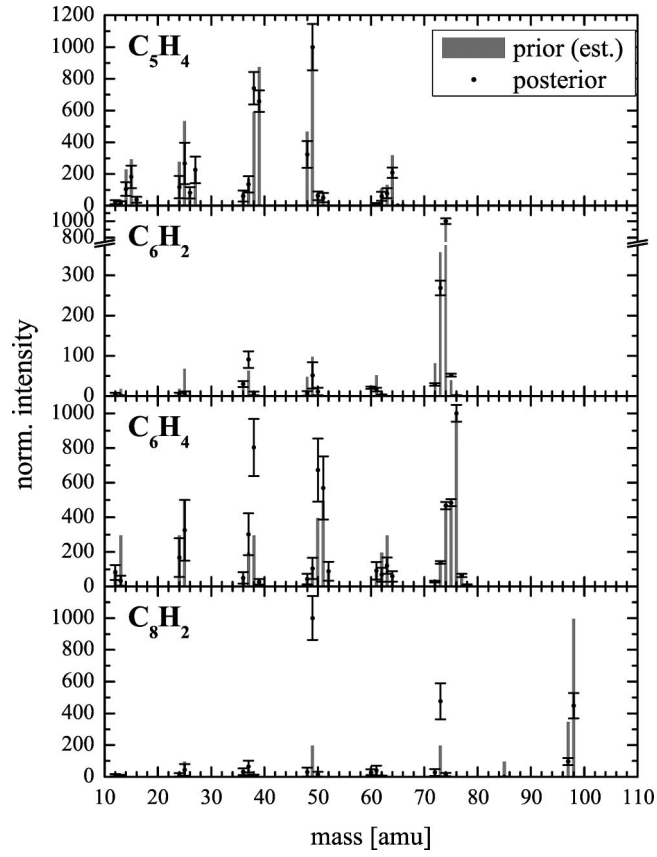

Figure 5. Prior and posterior CPs for C_5H_4, C_6H_2, C_6H_4, and C_8H_2. The prior CPs are estimated by comparison to known CPs of smaller molecules.

usually the most stable. Their formation is consistent with the work of Stefanović et al.,[21] who used IR spectrometry to detect aromatic compounds inside dust particles created in acetylene plasmas. However, we cannot rule out the presence of linear C_6H_6. The overall good agreement between posterior CPs and prior CPs from NIST data implies a small error margin for the determined concentrations ($\vec{x}$).

3. Prior CPs from Estimation. Figure 5 shows estimated prior CPs of C_5H_4, C_6H_2, C_6H_4, and C_8H_2 and corresponding posterior CPs. These CPs are most critical because only estimated prior CPs have been used and any differences between prior and posterior CPs are expected. The quality of these posterior CPs can be judged by two measures. First, the resulting error margins of the posterior CPs are a primary measure of their accuracy: a small error indicates that the measured data contain enough information so that the Bayes analysis yields a unique posterior CP and partial pressure; a large error indicates that the measured data are not informative. Second, the sensitivity of these posterior CPs to the change of the input data (additional species, different error margins) of the Bayes analysis.

The posterior CP of C_6H_2 exhibits rather small errors because (i) the mass spectrometer signals and thus the partial pressure of C_6H_2 are rather large and (ii) the temporal evolution of the partial pressure differs from other species. This makes the search for a solution of the CP and partial pressure of C_6H_2 unique. Consequently, the posterior CP of C_6H_2 is a reasonable estimate for its true CP.

The posterior CPs of C_8H_2, C_5H_4, and C_6H_4 exhibit rather large errors, because the partial pressures and hence also the corresponding signals are small with low signal-to-noise ratio.

To test the reliability of the posterior CPs, the analysis is repeated using a varying total number of considered species (adding C_3H_4, C_3H_6, and two linear C_6H_6 molecules). This analysis has shown that these posterior CPs remain very similar except that of C_5H_4. The C_5H_4 CP and its partial pressure varies strongly for different input parameters indicating that the measured data are not restrictive for determination of CP and partial pressure of C_5H_4.

We conclude that the posterior CPs of C_6H_4 and C_8H_2 are probably a good estimates of the true CPs and can be used until precise data is available in the literature. The posterior CP of C_5H_4 is very probably incorrect and its corresponding partial pressure is unreliable and very probably overestimated.

Summarizing, one can state that despite the crude estimate of the prior CPs, the data were restrictive enough to lead to posterior CPs with rather small error margins. In fact, most peaks exhibit only a small difference between prior and posterior CPs. The remaining differences are as follows:

The prior and posterior CPs of C_6H_2 differ for mass channels 25 and below. This is similar to C_4H_2 and may be again explained by a noncorrected mass transmission in the NIST C_4H_2 CP, which is used as a model for C_6H_2.

The posterior CP of C_6H_4 exhibits a maximum peak at 38 amu rather than at 76 amu as in the prior CP. The remainder of the posterior CP exhibits only small error margins.

The posterior CP of C_8H_2 exhibits the largest difference to the prior CP. The parent molecular peak (98 amu) is not the most intense peak in the posterior CP. Instead, the peak at mass 49 amu is dominant in the posterior CP. This change in the CP with increasing molecular size is common for larger hydrocarbon molecules: with increasing molecular size, the probability for dissociative ionization at a CC bond outnumbers the dissociative ionization at a CH bond or direct ionization.

We assume that the resulting absolute partial pressures of these species (except C_5H_4) will have an accuracy of about a factor of 2. We remind the reader that larger molecules (mass > 103 amu) may still contribute to the mass spectra shown in Figure 2b. We have neglected this contribution because of very low signal intensities in the mass spectra above 103 amu. Consequently, the partial pressures of these three species are probably an upper density limit.

B. Quantitative Analysis of the C_2H_2 Plasma Chemistry. The temporal evolution of absolute partial pressures is analyzed. The results are compared to previous conclusions based on a qualitative analysis of the mass spectra.[14]

The densities of hydrocarbon molecules prior to plasma ignition at $t = 0$ s are analyzed in a separate Bayes analysis, which considers only the precursor species C_2H_2, C_2H_4, Ar, and acetone and residual gases in the mass spectrometer (N_2, O_2, H_2O, and CO_2). Calibration measurements are available for all these species. The corresponding partial pressures of C_2H_2, C_2H_4, and acetone are indicated in the following at $t = 0$ s.

The densities of hydrocarbon molecules and acetone at different times t after plasma ignition are shown in Figure 7. The background species (N_2, O_2, H_2O, and CO_2) are not shown since they are just residual gases in the mass spectrometer and their partial pressures do not change after plasma ignition. They do not participate in the plasma chemistry.

With the exception of C_2H_2, C_2H_4, and acetone, all partial pressures follow a typical behavior: after plasma ignition, new species are formed with a partial pressure rising until a maximum, followed by a decrease due to the consumption of the precursor gas reservoir in the reactor. After several seconds, the partial pressures reach a saturation level due to the balance between precursor inflow and losses due to dissociation, chemical reactions, or pumping.

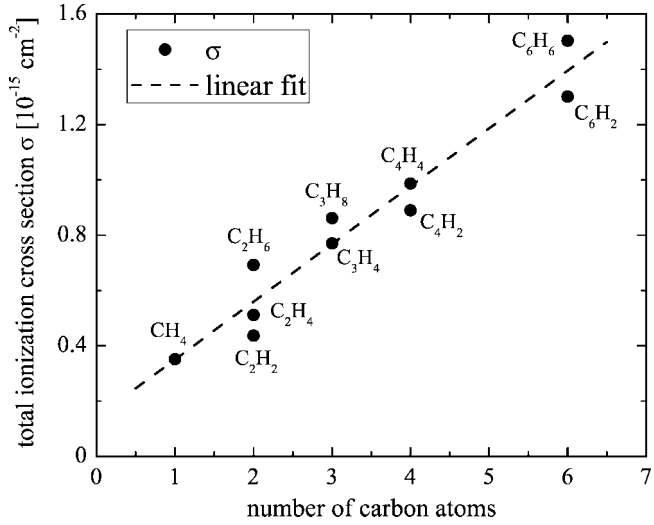

Figure 6. Scaling of the total ionization cross section of an organic molecule in dependence of the number of carbon atoms in that molecule. The dashed line is used to interpolate the total ionization cross section for those molecules for which the cross sections is not measured.

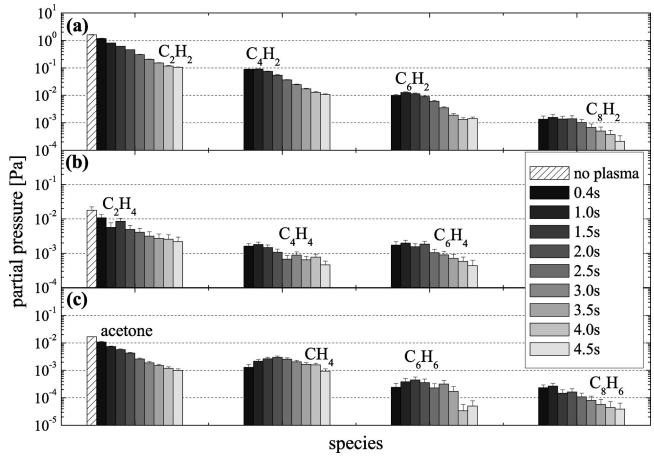

Figure 7. Temporal evolution of the partial pressure of $C_{2n}H_2$ species (a), of $C_{2n}H_4$ species (b), and of acetone, methane, and aromatic compounds (c).

The very similar temporal evolution of C_2H_2 (Figure 7a), C_2H_4 (Figure 7b), and acetone (Figure 7c) indicates an intimate link among these species. They exhibit the highest density prior to plasma ignition, and the density drops sharply after plasma ignition. The similar behavior of C_2H_2 and acetone is reasonable because the standard acetylene is dissolved in acetone in the gas bottle for stabilization. More interesting, we conclude that also C_2H_4 represents a main acetylene impurity with a partial pressure of approximately 0.18 Pa (ca. 1% of the C_2H_2 partial pressure) at time $t = 0$ s (no plasma). The Bayesian analysis is able to uniquely identify this impurity in the feed gas, although the CP of C_2H_4 overlaps with the CPs of C_2H_2, of N_2, and of CO. The influence of C_2H_4 on the plasma chemistry is discussed below. The additional impurity acetone leads to an increased production of H_2, CH_4, and CO. No other changes could be detected. This is discussed in detail in the appendix.

We discuss the reaction products and their chemistry in three separate groups, namely $C_{2n}H_2$ molecules, C_nH_4 molecules, and aromatic compounds.

1. Partial Pressures and Formation of $C_{2n}H_2$ Molecules. Figure 7a shows the temporal evolution of the partial pressure of $C_{2n}H_2$ ($n = 2-4$) molecules. C_4H_2 and C_6H_2 are dominant hydrocarbon products in the plasma with maximum partial pressures of 0.1 and 0.013 Pa, respectively. C_8H_2 reaches a maximum partial pressure of 0.0018 Pa. The maxima appear at later times for larger molecules. This observation is in agreement with findings in the literature[9,14] stating that $C_{2n}H_2$ ($n = 2-4$) molecules are formed via C_2H-induced polymerization: at first, C_2H is created via electron impact dissociation of the source gas C_2H_2:[22]

$$C_2H_2 + e^-(E_{el} \geq 7.5\ eV) \rightarrow C_2H + H + e^- \qquad (2)$$

Then, polymerization proceeds through consecutive steps via addition of C_2H radicals to $C_{2n}H_2$ molecules, starting with acetylene:

$$C_{2n}H_2 + C_2H \rightarrow C_{2n+2}H_2 + H \qquad (3)$$

This polymerization sequence induces a time delay between consecutive reaction steps. Two seconds after plasma ignition, the densities start scaling with the C_2H_2 signal. An equilibrium between production and losses inside the plasma volume is reached.

The first polymerization step involving C_2H_2 molecules and C_2H radicals is well studied revealing a rate constant of $k_1 = 1.3 \times 10^{-10}$ cm^3 s^{-1} with C_4H_2 being the dominant product.[23] The rate constants of consecutive polymerization steps are not known, but a similar delay of 0.3−0.4 s between the appearance of the maxima and the similar drop of the density between the two (see Figure 7a) indicates that the rate constants are comparable to k_1. This hypothesis has been previously verified using a simple rate equation model.[14]

2. Partial Pressures and Formation of C_nH_4 Molecules. In the following, we regard the plasma chemistry of C_nH_4 molecules and discuss the formation pathways of C_4H_4 in detail. Figure 7b shows the temporal evolution of the partial pressures of C_2H_4, C_4H_4, and C_6H_4 with maxima of 0.018, 0.0019, and 0.0024 Pa, respectively. The temporal evolution of CH_4 is shown in Figure 7c, and its maximum partial pressure is 0.003 Pa.

The density maximum of C_4H_4 appears very rapidly after plasma ignition. The maximum partial pressure of C_4H_4 is reached at the same time as that of C_4H_2 (cf. Figure 7, panels a and b), which is produced in a single reaction step (cf. 3, $n = 2$) as described before. This is surprising because reactions of C_2H_2 or C_4H_2 with C_2H or H cannot produce C_4H_4 in a fast, single reaction step. This suggests that some other reaction contributes to the fast initial formation of C_4H_4. As an explanation, we have suggested previously mutual anion-cation recombination or vinylidene reactions as a possible source reactions for C_4H_4 species.[14] However, with the knowledge that C_2H_4 is a significant impurity in the C_2H_2 gas, we disregard this hypothesis. C_4H_4 formation proceeds very probably through reaction

$$C_2H_4 + C_2H \rightarrow C_4H_4 + H \qquad (4)$$

with a rate constant of $k = (1.13 \pm 0.14) \times 10^{-10}$ cm^3 s^{-1}.[24] This reaction pathways has been investigated by intentionally adding additional 1% of C_2H_4 to the feed gas supply and monitoring the parent masses of C_2H_4 (28 amu) and of C_4H_4 (52 amu) respectively. The addition of C_2H_4 does not change the overall plasma chemistry since the intensities of the molecular masses of $C_{2n}H_2$ remain unchanged. Acetone-free C_2H_2 is used as precursor gas for this test to avoid strong contributions of CO to the signal at mass 28 amu.

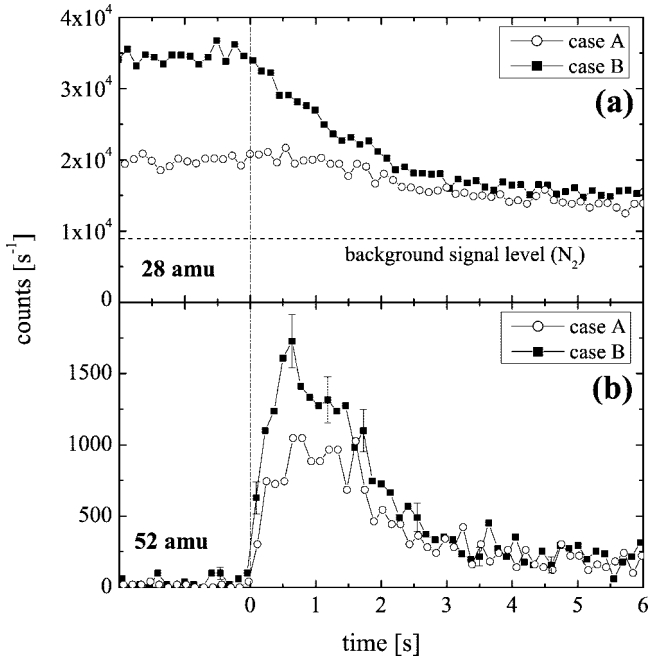

Figure 8. Temporal evolution of the mass 28 (a, parent peak of C_2H_4) and mass 52 signal (b, parent peak of C_4H_4). Two cases are considered: (case A, open circles) acetylene containing 1% C_2H_4 as impurity is used as precursor gas; (case B, solid squares) an additional flow of 1% C_2H_4 is intentionally added to the acetylene flow, which contains already 1% C_2H_4 as impurity.

Figure 8a shows the change of the signal at mass 28 amu using either solvent-free C_2H_2 containing 1% of C_2H_4 impurity (case A) or the same precursor mixture, but with an additional 1% C_2H_4 flow (case B). The intensity prior to plasma ignition for case A is larger due to the additional C_2H_4 in the precursor flow. After plasma ignition, the signal drops within 1−2 s in case B due to the fast decomposition of C_2H_4 into C_2H_2 and H_2 via electron collisions (threshold energy 5.8 eV). A convergence of the intensities in case A and case B occurs 2−3 s after plasma ignition. The fact that the C_2H_4 density in the later stage of the discharge is almost identical in both cases indicates that C_2H_4 is formed in the plasma even without being introduced as an impurity in the bottle.

To investigate the influence of the additional flow of C_2H_4 on the formation of C_4H_4, we investigate the signal variation at mass 52 amu corresponding to the molecular mass of C_4H_4. A signal variation at this mass directly reflects a density change of C_4H_4 because larger hydrocarbons have only a negligible contribution to it. Figure 8b shows the intensity changes at mass 52 amu for cases A and B. The C_4H_4 intensities are below the detection limit prior to plasma ignition and rise quickly afterward. The intensity in case B has a steeper increase and its maximum is 50% to 100% larger compared to case B within 2−3 s after plasma ignition. Afterward, the intensities of case A and B converge and remain the same until the plasma is switched off. Interestingly, the 2−3 s period of excess production of C_4H_4 after plasma ignition is synchronous to the fast decomposition of C_2H_4 in Figure 8a. This corroborates that the suggested reaction channel given in eq 4 is a source of C_4H_4.

An increase of the signal intensities in case B is also observed at the masses 16 amu (molecular mass of CH_4), 39 amu (molecular mass of C_3H_4), 64 amu (molecular mass of C_5H_4), 76 amu (molecular mass of C_6H_4), and 78 amu (molecular mass of C_6H_6). However, the signal increase is the less pronounced the higher the mass is. This is explained by the necessity of

second and third order reactions for the formation of these larger molecules since the contribution of an additional flow of C_2H_4 is distributed over many reaction channels. The details of the C_2H_2 chemistry as being altered by C_2H_4 addition will be published elsewhere.

3. Partial Pressures and Formation of C_6H_6 and C_8H_6 Molecules. For C_6H_6, it is not a priori known whether linear, aromatic, or both structures are formed in the C_2H_2 plasma. To test which isomer is present in our experiment, we have implemented the CPs of linear C_6H_6 (1,4- and 2,4-hexadiyne) and the CP of aromatic C_6H_6 (benzene) in our analysis. Three cases were considered in different runs of Bayes analysis: only linear C_6H_6, only aromatic C_6H_6, and both structures simultaneously. By comparing the results it is revealed that the sum of the linear and aromatic C_6H_6 partial pressures remains the same regardless of which case is considered. Since the CPs of C_6H_6 isomers are rather similar, we are not able to distinguish benzene form linear isomers. Consequently, we show only the total C_6H_6 partial pressure without specifying the exact C_6H_6 isomer. The CP of phenylacetylene is used for C_8H_6. No additional tests have been performed to look for other C_8H_6 isomers.

Figure 7c shows the temporal evolution of the partial pressures of C_6H_6 and C_8H_6 (together with acetone and CH_4). The partial pressures of C_6H_6 and of C_8H_6 reach maximum values of 6×10^{-4} and 3×10^{-4} Pa, respectively. The maximum density of C_6H_6 is delayed with respect to the maximum density of C_4H_2 (Figure 7a), indicating that several reaction steps are involved in its formation. As already mentioned in the previous section, the signal at molecular mass of C_6H_6 (78 amu) is influenced by addition of C_2H_4 to the precursor gas. It indicates that C_2H_4 or some following products are involved in the formation of either linear or aromatic C_6H_6.

C_8H_6 is very quickly produced in our experiment. The maximum density is reached in the first 0.2 s after plasma ignition (see Figure 7c). We have already shown that C_8H_6 is partly produced in surface reactions of C_2H radicals with adsorbed species on the reactor walls, originating from previous depositions. This hypothesis was tested by applying an intermediate cleaning step between experiments. Starting with a clean reactor, the molecular mass of C_8H_6 (102 amu) exhibits a slower buildup and a lower overall maximum density compared to measurements in a precoated reactor. More details can be found in ref 14.

C. Comparison of Partial Pressures with Literature Data. The knowledge of absolute partial pressures of 22 species gives us the unique opportunity to compare the results with data from the literature on a quantitative basis. For this, we chose experiments by Deschenaux et al.[11] and the modeling by de Bleecker et al.[9,15]

Deschenaux et al. investigated a pure C_2H_2 capacitively coupled rf plasma. They used a total pressure of $p = 10$ Pa, a C_2H_2 gas flow of $\Phi_{C_2H_2} = 8$ sccm, and an output rf power of $P = 40$ W. They applied mass spectroscopy to detect positive and negative ions as well as neutrals. A qualitative comparison of their neutral mass spectrum with our reconstructed spectra shows good agreement, which indicates that the presence of argon and helium in our plasma does not significantly change the C_2H_2 plasma chemistry. In addition, we may imply that also their negative and positive ion spectra are representative for our plasma.

De Bleecker et al. developed a model to describe the experiment of Deschenaux et al. The model is a 1D fluid code, involving 55 different species (neutrals, radicals, ions, and electrons) and 140 reactions. The best match to the experimental

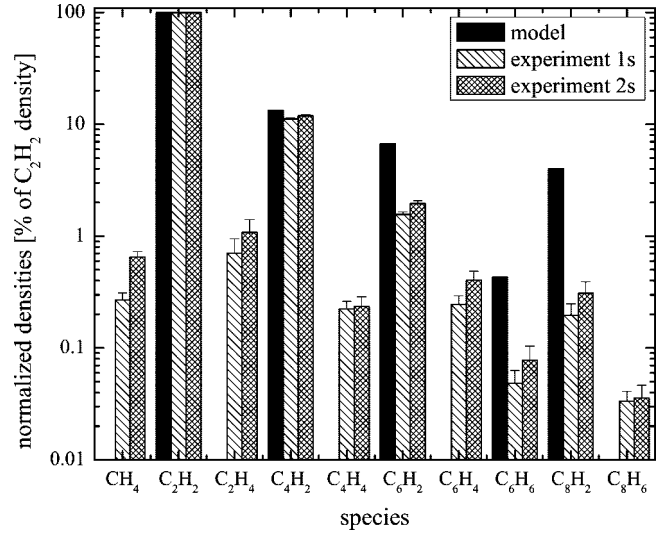

Figure 9. Comparison of the measured species densities (experiment) to the model values of De Bleecker et al.[15] (model). All densities are normalized to the C_2H_2 density.

results was achieved if the plasma parameters in the model were set differently to the actual parameters of the experiment: a total pressure of $p = 40$ Pa, a C_2H_2 gas flow of $\Phi_{C_2H_2} = 20$ sccm, and a coupled rf power of $P_c = 40$ W. The modeling yielded absolute densities of ions and neutrals.

De Bleecker et al. achieved very good agreement between the measured and modeled positive ion spectrum. This indicates that the model reproduces the positive ion chemistry very well and that the initial model assumptions are reasonable. However, a considerable disagreement was found if modeled and measured negative ion spectra are compared. The data of Deschenaux et al. show C_6H^- being the dominant ion, followed by $C_6H_2^-$, C_8H^-, and C_4H^- anions, whereas the model by de Bleecker et al. predicted monotonically decreasing $C_{2n}H^-$ anion densities with increasing n ($n = 1-12$). Apparently, the assumption that the dominant process for anion formation in the model is dissociative electron attachment to C_2H_2 followed by polymerization of negative $C_{2n}H^-$ ions by acetylene is either not valid or incomplete.

The discrepancy in the anion spectra between model and experiment can be explained by comparing our results to the modeled neutral species densities. This comparison is shown in Figure 9. The measured densities are given in hatched bars at times $t = 1$ and 2 s after plasma ignition. The model densities from refs 9 and 15 are shown as filled bars. Measured and modeled densities are normalized to the corresponding C_2H_2 density, which is set to 100%. It can be seen that the modeled densities of $C_{2n}H_2$ molecules, except of C_4H_2, exceed significantly our measured densities.

The discrepancies between model and experiment, namely (i) missing C_6H^-, $C_6H_2^-$, C_8H^-, and C_4H^- negative ions and (ii) too high densities of $C_{2n}H_2$ ($n > 1$) molecules, can be explained by an additional reaction pathway. We propose that $C_{2n}H_2$ ($n > 1$) molecules are effectively converted to large negative ions via dissociative electron attachment. It is well-known that vibrational excitation can enhance the reaction rate for dissociative electron attachment by several orders of magnitude.[25] Since $C_{2n}H_2$ molecules are formed in the plasma chemistry, they can be formed chemically activated with high vibrational excitation. Consequently, a high production rate of negative ions, which exceeds the production rate from ground-state acetylene, is probably realized in this way. This is also in

agreement with recent measurements of May et al.,[26] who have shown that the dissociative electron attachment cross section of C_4H_2 increases from 3 to 73 pm^2 by increasing the incident electron energy from 2.5 to 5.25 eV, which is the range of typical electron energies in CCP plasmas. The incorporation of the dissociative electron attachment reaction pathway into the model would thereby lead to a decrease of the $C_{2n}H_2$ densities and a simultaneous increase of the negative ion densities. As a result, the modeled densities and measured densities will better agree. This hypothesis is also consistent with the very rapid appearance of dust particles. The 2−10 nm big particles appear already at 250 ms after plasma ignition. The partial pressures of C_4H_2, C_6H_2, and C_8H_2 at $t = 200$ ms after plasma ignition are already 0.07, 0.006, and 7.3×10^{-4} Pa, respectively, which is approximately already a half of their maximal values.

Summarizing, we state that the dissociative electron attachment to $C_{2n}H_2$ ($n > 1$) molecules is probably the dominant source of negative ions in C_2H_2 plasmas and can explain the dominant tendency of C_2H_2 plasmas to dust particle formation.

VI. Conclusion

We have performed a quantitative analysis of the neutral plasma chemistry in a dust forming capacitively coupled argon/helium/acetylene discharge using time-resolved molecular beam mass spectrometry. Bayes statistics have been used to extract cracking patterns and partial pressures from the time-resolved mass spectrometric data. Twenty-two neutral species were identified and quantified. The cracking patterns of these species are obtained from calibration measurements, from the NIST database, or are estimated by comparison to other molecules. The Bayesian approach is also used to quantify cracking patterns which are not known a priori. The cracking patterns of C_6H_2, C_6H_4, and C_8H_2 are determined in this way and they can serve as good estimation, until precise data is published.

The most abundant products in our plasma are C_4H_2 and C_6H_2 molecules with maximum partial pressures of 0.1 and 0.013 Pa, respectively. The are produced, together with C_8H_2, in polymerization reactions of $C_{2n}H_2$ molecules with the C_2H radical.

C_2H_4 is identified as significant impurity in our acetylene gas. It constitutes approximately 1% of the acetylene density before plasma ignition and has a partial pressure of 0.018 Pa prior to plasma ignition. This molecule has not been considered in our previous qualitative analysis of the measured data. We have shown that C_2H_4 takes part in the formation of C_4H_4 molecule, most probably in a fast direct reaction with C_2H radical. The change of C_2H_4 partial pressure also affects the signal at molecular masses of other C_nH_4 and C_6H_6 molecules. The measured signals at mass 28 amu (molecular mass of C_2H_4) indicate that C_2H_4 is formed even in pure C_2H_2 plasma.

The maximum partial pressures of C_6H_6 and C_8H_6 are 6×10^{-4} and 3×10^{-4} Pa. The C_6H_6 partial pressure reaches its maximum rather late compared to the one of C_4H_2 indicating, that several reaction steps are involved in its formation. We could not distinguish between linear and aromatic isomers of C_6H_6 in our analysis. The maximum partial pressure of C_8H_6 is reached very quickly after plasma ignition, which is in agreement with our previous conclusion that it is mainly formed in surface reactions at the reactor wall.[14]

The quantitative results presented in this article can be used now to validate modeling results of C_2H_2 plasmas. We have performed a first rough comparison of our data to a similar measurement of Deschenaux et al. and to a recent model calculation performed by De Bleecker et al. The direct comparison of measured and modeled partial pressures (normalized to C_2H_2 density) shows that some loss channels for $C_{2n}H_2$ molecules are missing in the model. Additional dissociative electron attachment to these large (probably vibrationally excited) molecules results in their additional loss and can explain discrepancies in modeled negative ion densities and measured negative ion mass spectrum of Deschenaux et al. The negative $C_{2n}H^-$ ions resulting from these reactions are the most probable dust particle precursors in C_2H_2 plasmas.

Acknowledgment. The authors thank T. Schwarz-Selinger for providing the Bayes algorithm and V. Dose for his introduction and advice using Bayes methods. We thank A. Boegarts, K. de Bleecker, and M. Mao for many valuable discussions regarding the hydrocarbon chemistry in acetylene plasmas. We also thank M. Schulze for providing guidance in the dust forming experiments. We thank Norbert Grabkowski for his skillful technical assistance. The work is supported by the German Science Foundation in the framework of the graduate school 1051. Additional support is granted by the Ruhr-University Research School funded by Germany's Excellence Initintive [DFG GSC 98/1].

Appendix A: Analysis of Mass Spectra Using Bayesian Statistics

The details of the Bayes approach are presented in detail by Schwarz-Selinger et al.[16] and by Kang et al.[17] The most important steps of this approach are described in the following. First, we define a mathematical description of the mass spectra problem. The measured data are expressed as a vector $\vec{d}$ containing i peaks corresponding to the ions generated via ionization and fragmentation of collected neutrals in the ionizer of the mass spectrometer. The concentrations of stable neutrals in the plasma are expressed as a vector $\vec{x}$ containing s species. Here, we restrict ourselves to a reasonable set of species which are believed to be present in the gas mixture. Both vectors are connected by a matrix $\hat{C}$ containing the CP of each species. The CP matrix $\hat{C}$ consists of i rows, with each column corresponding to that part of the CP of species s contributing to the mass channels i. In our experiment, a large number of measured mass spectra are incorporated in a single analysis. If we use the index j for each new experiment, the mathematical description of the problem can be written as

$$\vec{d}_j = \hat{C}\vec{x}_j \tag{A1}$$

This equation can be solved by the least-squares method, which is equivalent to search for the maximum of the likelihood $p(\vec{d}_j|\vec{x}_j, \hat{C}, \hat{S}_j)$ for a given set of data $\vec{d}_j$ if the concentrations $\vec{x}_j$ and the CP matrix $\hat{C}$ are known. The entries in the data vector $\vec{d}_j$ may contain an error, which is incorporated in a matrix $\hat{S}_j$ containing the error ϵ_i of mass peak i in experiment j on the main diagonal. The likelihood is given as

$$p(\vec{d}_j|\vec{x}_j, \hat{C}, \hat{S}_j) \propto \exp\left[-\frac{1}{2}(\vec{d}_j - \hat{C}\vec{x}_j)^{\mathrm{T}}\hat{S}_j^{-2}(\vec{d}_j - \hat{C}\vec{x}_j)\right] \tag{A2}$$

The main goal is the determination of the species with unknown concentrations $\vec{x}_j$, which are assumed to be simultaneously present in all experiments $\vec{d}_j$ given a single CP matrix $\hat{C}$, which remains identical irrespective of the experiment. Such an approach is optimal for the analysis of time-dependent data, as will be presented below.

The least-squares method is best suited for overdetermined problems. In our case, however, some of the CP are not known or may contain large errors. The analysis of such ill-posed

problems can be performed by using Bayesian statistics. For this, the likelihood is inserted into the so-called Bayes-theorem[27] to gain an expression for the probability p of the concentrations $\vec{x}_j$ for a given set of data $\vec{d}_j$

$$p(\vec{x}_j|\vec{d}_j, \hat{C}, \hat{S}_j) = p(\vec{x}_j)p(\vec{d}_j|\vec{x}_j, \hat{C}, \hat{S}_j)/\text{Norm} \quad \text{(A3)}$$

Norm refers to a normalization constant, which is irrelevant for the search of the maximum of $p(\vec{x}_j|\vec{d}_j, \hat{C}, \hat{S}_j)$. By applying the Bayes theorem, a new probability $p(\vec{x}_j)$ is introduced, which corresponds to the prior for the concentrations $\vec{x}_j$. A prior contains a-priori information regarding the quantity of interest. In our case, we do not make any assumptions regarding the species concentrations and set this prior to $p(\vec{x}_j) = 1$.

In the case of CPs, however, prior information may exist since these values might be tabulated in databases or can directly be measured by using calibration experiments. This prior information is incorporated by using the marginalization rule: the likelihood is averaged over all possible CPs by weighting this average with the prior information $p(\hat{C})$

$$p(\vec{x}_j|\vec{d}_j, \hat{C}, \hat{S}_j) \propto \int p(\hat{C})p(\vec{d}_j|\vec{x}_j, \hat{C}, \hat{S}_j)\, dC \quad \text{(A4)}$$

The main advantage of this formulation of the problem is the fact that the final solution $p(\vec{x}_j|\vec{d}_j, \hat{C}, \hat{S}_j)$ depends not only on the actual measured data $\vec{d}_j$ but also on the CPs $\hat{C}$, which might be only known within a certain error margin. The treatment of the CPs and their error margin are therefore of key importance for the final solution. This will be discussed in the following.

1. Prior Information for the Cracking Pattern (CP). The prior for the CP matrix $p(\hat{C})$ is composed of the priors for individual CPs $p(\vec{c}_s)$ of species s via

$$p(\hat{C}) = \prod_s p(\vec{c}_s) \quad \text{(A5)}$$

The prior for a CP $p(\vec{c}_s)$ is further composed of the priors $p(c_{si})$ for a single mass peak i in CP $\vec{c}_s$ via

$$p(\vec{c}_s) = \prod_i p(c_{si}) \quad \text{(A6)}$$

Finally, the prior for a single mass peak i is given by a Gaussian using an expectation value μ_{si} and an error σ_{si}.

$$p(c_{si}) \propto \exp\left(-\frac{(c_{si} - \mu_{si})^2}{2\sigma_{si}^2}\right) \quad \text{(A7)}$$

The expectation values and errors are taken from databases or are determined in calibration experiments.

2. Solving the Problem. The species concentrations are determined by finding the maximum of the probability

$$p(\vec{x}_j|\vec{d}_j, \hat{C}, \hat{S}_j) \propto \int p(\hat{C})p(\vec{d}_j|\vec{x}_j, \hat{C}, \hat{S}_j)\, dC \quad \text{(A8)}$$

The maximum of p is equivalent to the maximum of $\ln(p)$. Thereby, the product of combined probabilities transforms to a sum over species$s$, mass channels i, and data sets j yielding a density functional

$$\sum_s \sum_i \ln p(c_{is}) + \lambda \sum_j \ln p(\vec{d}_j|\vec{x}_j, \hat{C}, \hat{S}_j) = \max \quad \text{(A9)}$$

The parameter λ represents a regularization parameter between likelihood and priors. The maximum is found by using a Markov chain Monte Carlo (MCMC) algorithm, which samples the complete solution space by varying all entries in the CPs, all concentrations, and the regularization parameter λ. The Monte Carlo algorithm samples the parameter space until the solution saturates. The sampling statistics provides then an estimate for the error of that solution.

The Bayes algorithm produces concentrations as well as posterior CPs including corresponding error margins. The posterior CPs might differ from prior CPs if the measured data contain enough information to allow for this deviation. If the data are not restrictive for such a deviation or if the prior CPs are already compatible with the data, the posterior and prior CPs are almost identical.

3. Retrieving Absolute Partial Pressures. The MCMC algorithm solves the problem using normalized data and cracking patterns. As a result, also normalized concentrations $\vec{x}$ are obtained, with $|\vec{x}| = 1$. For a direct comparison to the experiments, however, real partial pressures are needed. For the conversion from x_{species} to p_{species}, the calibration measurements are essential.

The partial pressure $p_{\text{species}}^{\text{calibration}}$ of a given species, as it is measured during calibration, is direct proportional to the (total) signal intensity $|\vec{d}^{\text{calibration}}|$ of the measured spectrum. This information is used to determine the partial pressure $p_{\text{species}}^{plasma}$ in the actual plasma experiment from the measured data $|\vec{d}^{\text{plasma}}|$ by

$$p_{\text{species}}^{\text{plasma}}(t) = p_{\text{species}}^{\text{calibration}}(t)\frac{|\vec{d}^{\text{plasma}}|}{|\vec{d}^{\text{calibration}}|} \quad \text{(A10)}$$

This approach works only for those species for which a known partial pressure can easily be adjusted in an calibration measurement (CH_4, C_2H_2, C_2H_2, Ar, N_2, and O_2). If no partial pressure information is available, i.e., in database spectra, an alternative method must be applied. Here, we chose an approach similar to threshold ionization mass spectrometry (TIMS)[28] for which the density of an unknown species is quantified by using the ratio of ionization cross sections and one known species density. In our case, we set the total ionization cross section of the species of interest σ_s in relation to the known total ionization cross section for acetylene $\sigma_{\text{acetylene}}$ and the known partial pressure $p_{\text{acetylene}}$. Then, the unknown partial pressure p_s can be calculated from the concentrations x, as determined by Bayesian analysis via

$$p_s(t) = p_{\text{acetylene}}^{\text{plasma}}(t)\frac{\sigma_{\text{acetylene}}}{\sigma_s}\frac{x_s(t)}{x_{\text{acetylene}}(t)} \quad \text{(A11)}$$

The error of the partial pressure is mainly determined by the error of $x_s(t)$ and of σ_s. The error of the total ionization cross section is in general 10% or better.

Appendix B: Contribution of Acetone to the Acetylene Plasma Chemistry

Acetone represents a significant impurity if acetylene dissolved in acetone is used as precursor gas. The qualitative analysis of the mass spectra revealed[14] that the presence of acetone has no influence on the densities of larger hydrocarbon molecules. This is now confirmed by the quantification of the acetone density and its comparison to the production of CO in the plasma: acetone is approximately 1% of the C_2H_2 partial pressure at the time $t = 0$ s (no plasma). Figure 10 shows that the consumption of acetone after plasma ignition is accompanied by a corresponding increase of the CO partial pressure. The slightly higher partial pressure of CO is within error for CO partial pressure and systematic error due to an only estimated ionization cross section of acetone (this error is not shown in Figure 10). It indicates that the CO group of acetone

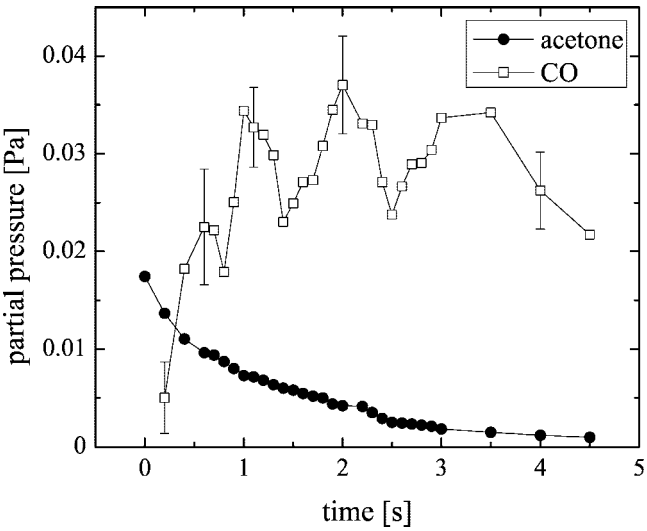

Figure 10. Temporal evolution of the acetone and CO partial pressures. The absolute value of the acetone partial pressure contains a systematic error of several 10%.

(CH_3COCH_3) is mainly preserved by splitting off methyl groups in the plasma dissociation. This can be tested by comparing plasmas from acetylene dissolved in acetone with acetone-free acetylene: the formation of methyl groups becomes visible as an increase of the CH_4 density compared to the case if acetone-free C_2H_2 is used. No CO formation is observed when acetone-free C_2H_2 is used as feed gas.

References and Notes

(1) Spears, K. G.; Robinson, T. J.; Roth, R. M. *IEEE Trans. Plasma Sci.* **1986**, *14*, 179.
(2) Selwyn, G. S.; Singh, J.; Bennet, R. S. *J. Vac. Sci. Technol.* **1989**, *A7*, 2758.
(3) Kortshagen, U.; Mangolini, L.; Bapat, A. *J. Nanopart. Res.* **2007**, *9*, 39.
(4) i Cabarrocas, P. R.; Chaâbane, N.; Kharchenko, A. V.; Tchakarov, S. *Plasma Phys. Control. Fusion* **2004**, *46*, B235.
(5) Kovačević, E.; Stefanović, I.; Berndt, J.; Pendelton, Y. J.; Winter, J. *Astrophys. J.* **2005**, *623*, 242.
(6) Bouchoule, A. *Dusty Plasmas: physics, chemistry and technological impacts in plasma processing*; John Wiley & Sons: New York, 1999.
(7) Howling, A. A.; Sansonnens, L.; Dorier, J. L.; Hollenstein, C. *J. Phys. D* **1993**, *26*, 1003.
(8) Bhandarkar, U. V.; Swihart, M. T.; Girshick, S. L.; Kortshagen, U. R. *J. Phys. D* **2000**, *33*, 2731.
(9) Bleecker, K. D.; Bogaerts, A.; Goedheer, W. *Phys. Rev. E* **2006**, *73*, 026405.
(10) Hong, S.; Berndt, J.; Winter, J. *Plasma Sources Sci. Technol.* **2003**, *12*, 46.
(11) Deschenaux, C.; Affolter, A.; Magni, D.; Hollenstein, C.; Fayet, P. *J. Phys. D* **1999**, *32*, 1876.
(12) Schulze, M.; von Keudell, A.; Awakowicz, P. *Appl. Phys. Lett.* **2006**, *88*, 141503.
(13) Schulze, M.; von Keudell, A.; Awakowicz, P. *Plasma Sources Sci. Technol.* **2006**, *15*, 556.
(14) Benedikt, J.; Consoli, A.; Schulze, M.; von Keudell, A. *J. Phys. Chem. A* **2007**, *111*, 10453.
(15) Bleecker, K. D.; Bogaerts, A.; Goedheer, W. *Appl. Phys. Lett.* **2006b**, *88*, 151501.
(16) Schwarz-Selinger, T.; Preuss, R.; Dose, V.; von der Linden, W. *J. Mass Spectrom.* **2001**, *36*, 866.
(17) Kang, H.; Preusss, R.; Schwarz-Selinger, T.; Dose, V. *J. Mass Spectrom.* **2002**, *37*, 748.
(18) *NIST Mass Spec Data Center, S.E. Stein, director, NIST Chemistry WebBook, NIST Standard Reference Database Number 69*; National Institute of Standards and Technology: Gaithersburg MD, 2005; Chapter Mass Spectra, http://webbook.nist.gov.
(19) Kim, Y.-K. Irikura, K. K. Rudd, M. E. Ali, M. A. Stone, P. M. Chang, J. Coursey, J. S. Dragoset, R. A. Kishore, A. R. Olsen, K. J. Sansonetti, A. M. Wiersma, G. G. Zucker, D. S. Zucker, M. A. *Electron-Impact Ionization Cross Section for Ionization and Excitation Database (version 3.0)*; National Institute of Standards and Technology: Gaithersburg, MD, 2004; http://physics.nist.gov/ionxsec, 2008, May 6th.
(20) Schram, B. L.; van der Wiel, M. J.; de Heer, F. J.; Moustafa, H. R. *J. Chem. Phys.* **1966**, *44*, 49.
(21) Stefanović, I.; Kovačević, E.; Berndt, J.; Pendleton, Y.; Winter, J. *Plasma Phys. Control. Fusion* **2005**, *47*, A179.
(22) Janev, R.; Reiter, D. *Phys. Plasmas* **2004**, *11*, 780.
(23) Laufer, A. H.; Fahr, A. *Chem. Rev.* **2004**, *104*, 2813.
(24) Vakhtin, A. B.; Heard, D. E.; Smith, I. W. M.; Leone, S. R. *Chem. Phys. Lett.* **2001**, *348*, 21.
(25) Christophorou, L. G. *Environ. Health Persp.* **1980**, *36*, 3.
(26) May, O.; Fedor, J.; Ibanescu, B. C.; Allan, M. *Phys. Rev. A* **2008**, *77*, 040701.
(27) Sivia, D. *Data Analysis: A Bayesian Tutorial*; Oxford University Press: New York, 1996.
(28) Benedikt, J.; Agarwal, S.; Eijkman, D. J.; Vandamme, W.; Creatore, M.; van de Sanden, M. C. M. *J. Vac. Sci. Technol. A* **2005**, *23*, 1400.

JP8042413